Reply to comments by referee #2

We appreciate the time and care the referee took to review the manuscript. The valuable suggestions and comments will be addressed below. The referee's comments are highlighted in blue.

Major comments:

Ice crystal habit, size and smooth crystal fraction (SCF) is inferred from the halo observations by matching the observations at different viewing angles to simulations. However, it is not shown how the halo properties change with habit, size and SCF. I do not believe this is described in the other two parts of the series. I suggest using the LUT to show how the observations vary systematically with habit, size and SCF. I suggest the investigations of sensitivities to size and SCF focus on the plate and column aggregate, as these appear to match the data mostly while yielding quite different results on SCF as seen in Fig 4.

We appreciate this suggestion and added the following paragraph accompanied by an additional figure to illustrate how the halo properties, in this case represented by the 22° and 46° halo ratio, depend on ice crystal shape, effective radius and smooth crystal fraction (SCF):

"Figure 1 illustrates how the properties of the 22° (upper panel) and 46° halo (lower panel), represented here by their respective halo ratio, vary with effective crystal radius r_{eff} and smooth crystal fraction (SCF). A halo ratio of 1 is considered as threshold for a visible halo display, indicated by the white contour. Below this value, the halo features are assumed to vanish compared to the background illumination. The key take away from this figure is that column-shaped crystals (solid columns, aggregates of 8-element columns, solid bullet rosettes) produce the most pronounced 22° halo, i.e. the largest halo ratio for a given smooth crystal fraction and effective radius. To produce a comparable 22° halo ratio, plate-like crystals (plates, 5-element, and 10-element aggregates of plates) need a much larger amount of smooth crystals, which implies a significantly larger 46° halo ratio compared to columnar crystals. Ice crystals with hollow base (hollow column, hollow bullet rosette) result in 22° halo ratios ranging between the values for columnar and plate-like crystals, however they do not produce a 46° halo since the cavity prevents the necessary raypath."

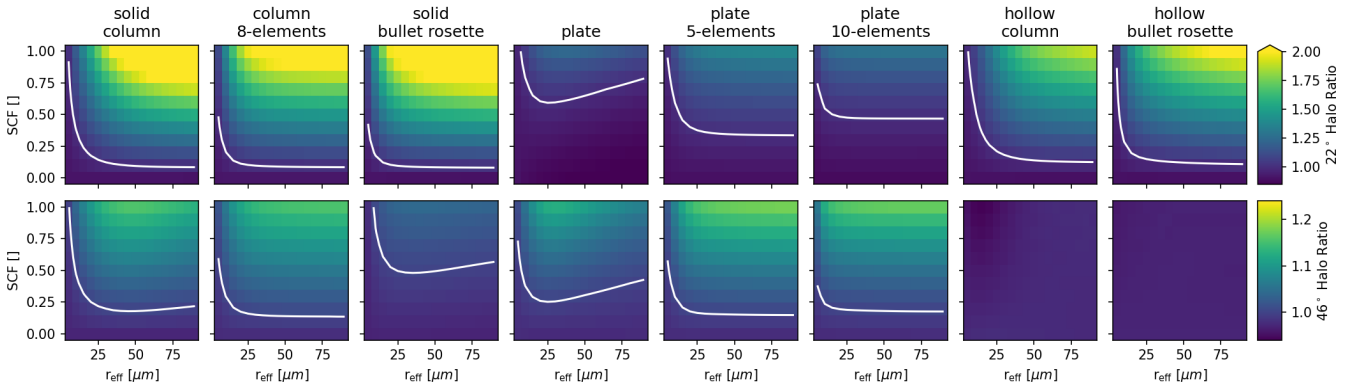

Figure 1. Sensitivity of the halo features, represented here by the 22° (upper panel) and 46° halo ratio (lower panel), to ice crystal shape, effective radius (x-axis), and smooth crystal fraction (SCF) (y-axis) based on the look-up tables (LUTs) used for the retrieval. These features are a selection of the full LUT for a wavelength of 618 nm, SZA = 40°, AOT = 0.25, COT = 1.0, and image segment no. 1 (cf. Forster et al. (2020), Fig. 3b). The white contour lines mark the threshold assumed here for a visible 22° or 46° halo at halo ratio HR = 1.

The retrieval procedure needs to be explained more clearly.

We rephrased the corresponding paragraphs to clarify the retrieval procedure and added a flow chart to help visualize the retrieval steps. The specific comments should all be addressed in this revised version. Responses to the individual questions are provided below.

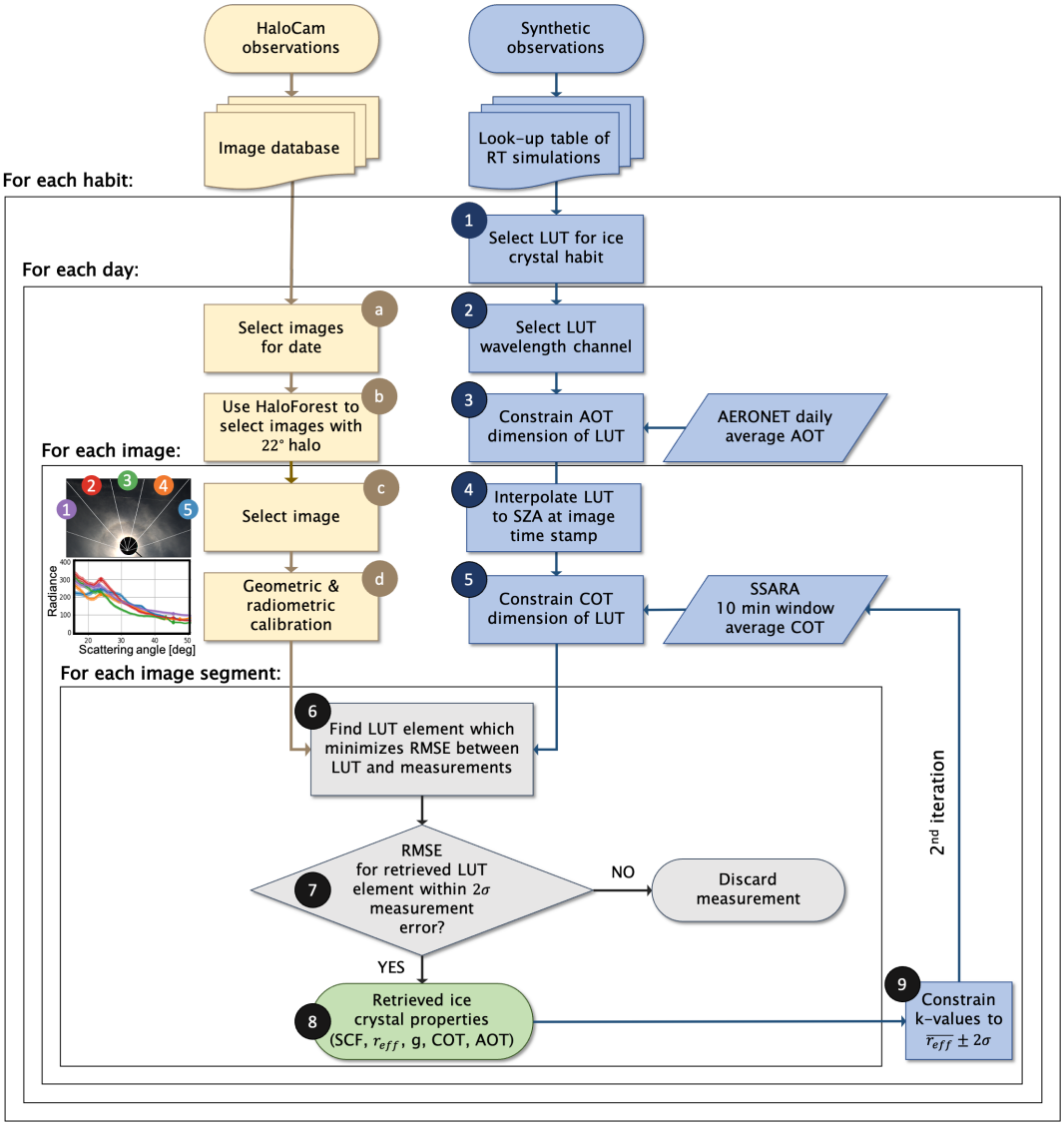

Figure 2. Flow chart visualizing the individual steps of retrieving representative ice crystal properties by finding the best match between HaloCam observations (yellow) and a look-up table (LUT) of radiative transfer simulations (blue).

"The retrieval was performed as illustrated in Fig. 2. The left (yellow) branch of the flow chart describes the processing of the HaloCam images, starting with (a) selecting images from the database for a specific day and (b) filtering them for a visible 22° halo using HaloForest (Forster et al., 2017). Looping over this filtered database, an

image is selected (c), calibrated (d) as described in Forster et al. (2020) and the retrieval is performed for each of the five image segments separately. A sample HaloCam$_{\mathrm{RAW}}$ image is shown here for illustration with the five image segments indicated and the corresponding radiance distributions as a function of scattering angle below. Each of the image segments is centered around the relative azimuth angles $\varphi_{\mathrm{center}} = 120°, 150°, 180°, 210°, 240°$ as listed in Table 2. Pre-processing of the synthetic observations from a LUT of radiative transfer simulations is represented by the right (blue) branch in Fig. 2 (steps 1 through 5), followed by the actual retrieval (steps 6 through 8):

1. For each ice crystal habit, the respective LUT was selected.
2. The LUT was further constrained to the wavelength representative for the image channel, here 618 nm.
3. **In a next step, the AOT dimension of the LUT was constrained using AERONET sunphotometer observations, interpolated to 618 nm. Since AERONET's AOT can only be measured during clear sky, the values during the observation of the halo display were estimated to range around the daily mean AOT within a 2σ confidence interval. The AOT dimension of the LUT was then constrained to the interval $[\overline{AOT} - 2\sigma, \overline{AOT} + 2\sigma]$. As an example, for 21 April 2016 the AOT dimension was allowed to range within 0.08±0.04 (cf. Fig. 3).**
4. Then, for each HaloCam$_{\mathrm{RAW}}$ image, the LUT was interpolated to the SZA corresponding to the image time stamp.
5. For each HaloCam$_{\mathrm{RAW}}$ image time stamp, the COT dimension of the LUT was constrained in addition. Sun photometer measurements using SSARA's high temporal resolution of 1 s were used to find a representative COT interval for each time step of halo observations. The COT was derived from SSARA's total optical thickness observations by subtracting AERONET's AOT and correcting the resulting apparent COT for the enhanced forward scattering by ice crystals according to Eq. B5 using the so-called k-value. For a fixed instrument field-of-view and for a given ice crystal shape, the k-value depends primarily on the ice crystal size (cf. Appendix B1.2) and was computed for the LUT's minimum and maximum effective radii of 5 and 90 μm as an initial guess. The representative COT interval was then determined by computing the average COT within a 2σ confidence interval over a 10 min time window (±5 min around the observation time stamp) to account for the slightly different pointing directions $\Theta = 0°$ (sun photometer) and $\Theta = 22°$ (halo display) in combination with the unknown wind direction.
6. For the retrieval, each of the five averaged radiance distributions measured with HaloCam$_{\mathrm{RAW}}$ was compared to the LUT elements with the respective viewing geometry. The residuum between measurements and LUT is quantified by the root mean squared error (RMSE), which is calculated by

$$\mathrm{RMSE} = \sqrt{\sum_{i=1}^{n} \frac{(L_{\mathrm{meas,i}} - L_{\mathrm{LUT,i}})^2}{n}}. \tag{1}$$

   using the measurements $L_{\mathrm{meas,i}}$ and LUT elements $L_{\mathrm{LUT,i}}$ within the considered scattering angle range and averaged over the number of elements n.
7. The LUT element with the minimum RMSE, averaged over the scattering angle range, represents the best match for the cirrus optical and microphysical properties.

$$\mathrm{RMSE} \leq \sum_{i=1}^{n} \frac{2\sigma_{\mathrm{L,meas,i}}}{n}. \tag{2}$$

   In case the average RMSE between LUT and measurements exceeds the 2σ measurement uncertainty, the measurements are discarded from the retrieval. This occurs for example for highly inhomogeneous scenes or cirrus properties outside the LUT.
8. The resulting smooth crystal fraction (SCF), effective radius r_{eff}, asymmetry factor g, cirrus optical thickness (COT), and aerosol optical thickness (AOT) are considered representative optical properties for the cirrus cloud region captured by the respective HaloCam image segment.

9. A second iteration of the retrieval is performed starting from step 5 to further constrain the COT dimension of the LUT. Using the retrieved effective radii for the five image segments, the minimum and maximum k-values are determined by the effective radius averaged over all image segments $\overline{r_{\mathrm{eff}}}$ within a 2σ confidence interval: $\overline{r_{\mathrm{eff}}} \pm 2\sigma$. This constrained range of k-values then translates to a further constrained COT dimension of the LUT.

"

Specifically: on page 8 you say that cases with RMSE values below 2-sigma measurement uncertainty are "considered possible solutions", while "the LUT element with the minimum RMSE represents the best match." How are the possible solutions used? Isn't only the best match considered the retrieved parameter set? Are there instances where the lowest RMSE is not lower than the 2-sigma measurement uncertainty and thus the retrieval fails?

Thank you for pointing this out. We rephrased the sentences for clarification. Changes are highlighted in red in the paragraph above.

The RMSE values are not very useful without a reference point, so please give a representative value of this 2-sigma measurement uncertainty. Alternatively or additionally, RMSE values could be normalized by the 2-sigma measurement uncertainty. The range of RMSE values in Fig 3 is quite broad, so is the 2-sigma measurement uncertainty quite large? Maybe I am not interpreting the RMSE values in Fig 3 correctly and these are not only for the 'best match' cases? If so, please explain in the text.

The 2σ radiometric measurement uncertainty depends on the measured radiance values and will be different for every time step. Typical values are e.g. 10 $\mathrm{mW\,m^{-2}nm^{-1}sr^{-1}}$ for a measured radiance of 220 $\mathrm{mW\,m^{-2}nm^{-1}sr^{-1}}$, which corresponds to an absolute radiometric response of about 4.5% as provided in Tab. 3 (Forster et al., 2020). Since the retrieval is applied to each time step separately, the same 2σ threshold and range of $L_{\mathrm{meas,i}}$ will be the reference to determine the best matching look-up table element. Normalizing the RMSE, would only change the x-coordinate of Fig. 4, but would not change how the RMSE values compare between the different ice crystal shapes. Since an additional reference point or normalization would not change the results of the retrieval, we decided to leave it as is.

Then in Figure 3, the AOD differs between the results for different habits, but it was explained that the AOT is constrained by clearsky observations before or after the cirrus observations, so I do not understand why this varies with habit?

The AOT is constrained to an interval between $\pm 2\sigma$ of the average AOT for clearsky observations before and/or after the halo observation. Since it can only be measured during clea sky, we consider this the best estimate for the halo observations. Depending on the single scattering properties of the selected ice crystal habit, the best matching LUT element might correspond to a combination of COT and AOT with slightly different values, within their respective intervals. **Changes are highlighted in bold font in the paragraph above**.

On page 7, line 13, it is stated that "the LUT was also constrained to SSARA's COT measurements within a 2-sigma confidence interval averaged over a ±5 min time interval." I am not sure what is meant here. I assume the COT within the LUT that matches most closely to the mean SSARA's COT is used, but it is not clear how the 2-sigma confidence interval is used.

Only halo observations corresponding to COT values within this interval were considered. Amongst these observations, the best match was selected. The rest of the observations is excluded from the retrieval. Changes are highlighted in teal font in the paragraph above.

On page 13, the sensitivity study is described and it is stated that "the LUT was modified by multiplication with a slope". But what specifically was multiplied? And with a slope with respect to what? Please clarify. Also, does the modified LUT also lead to a different SCF?

We appreciate the feedback and modified the section in the manuscript to better explain the procedure. The retrieved SCF remains mostly unaffected by using the modified LUT for the retrieval, except for the urban aerosol case which slightly changed the retrieved SCF for plates, 5-element and 10-element plates as described in the changes below.

"To investigate the sensitivity of the retrieval to different aerosol types, we would ideally compute new LUTs. Since computing a new LUT would require several weeks computation time on MIM's high performance computing cluster for each new aerosol type and the radiance at each scattering angle would basically only differ by a multiplicative factor, we repeated the retrieval with a modified LUT to estimate the effect of these approximations. The LUT was modified by multiplication with a factor for each scattering angle, which is representative for the amount and the sign of the bias introduced by the approximations. The multiplicative factor for each scattering angle in the LUT, which we refer to as "slope" in the following, was computed by the ratio between two radiance distribution, simulated with DISORT: One "reference" radiance distribution using the continental average aerosol type and one "modified" radiance distribution for each of the aerosol types: continental clean, continental polluted, and urban. In addition, a slope was generated by computing the ratio between a "reference" radiance distribution accounting for HaloCam$_{\mathrm{RAW}}$'s full spectral response (cf. solid red line in Fig. B3) and a "modified" radiance distribution based on HaloCam$_{\mathrm{RAW}}$'s representative wavelength of 618 nm for the red channel (cf. dashed red line in Fig. B3). These slopes were computed for each of the eight ice crystal habits assuming a representative atmospheric setup: COT = 0.8, AOT = 0.1, and a SCF of 30% for columnar crystals, 60% for hollow column crystals, and 70% for plate-like crystals.Table 4 shows the results of the best matching habit for each day retrieved with the modified LUT. The best matching habit changed slightly for the different modifications of the LUT but only within the plate-like or column-like crystal groups. The ice crystal plates remain the overall best-matching habit in the considered scattering angle range. The retrieved SCF in Table 3 remained mostly unaffected by using the modified LUT for the retrieval. Only for the urban aerosol case, the retrieved SCF for plates changed from $(80 \pm 10)\,\%$ to $(70 \pm 10)\,\%$, for 10-element plates from $(70 \pm 10)\,\%$ to $(80 \pm 10)\,\%$ and for 5-element plates from $(70 \pm 20)\,\%$ to $(60 \pm 20)\,\%$. "

In section 3.2 the 46 degree halo is simulated, but it is unclear what the SCF and size is used here, i.e. in Figs 6 and 7.

Appyling the retrieval to halo observations averaged over a whole day is the best approach to answer the question whether a (faint) 46° halo was present during the observations but yields, as expected, different results compared to applying the retrieval to individual observations and then averaging the retrieved cirrus properties. For the first approach, varying AOT and COT values over the course of the observation period cannot be accounted for, however the retrieved SCF and effective radius are strongly correlated with these values. This retrieval approach can therefore only help to constrain the particle shape but might induce a bias in the retrieved SCF and effective radius. For this reason we did not mention these values here to avoid the misunderstanding that those were the final retrieval results. We added the following explanation to the manuscript and for the sake of completeness, the ice crystal properties used for the DISORT simulations in a footnote.

"As mentioned above, applying the retrieval to HaloCam observations, which were averaged over a whole day, yields only qualitative results that help us confirm which ice crystal shape best matches the region both of the 22° and 46° halo. Since it does not allow for the retrieved cirrus and aerosol optical thickness to follow their natural temporal fluctuation, the retrieved smooth crystal fraction and ice crystal radius might get biased[1]. We therefore repeated the quantitative retrieval as described in Section 3.1 for the individual HaloCam$_{\mathrm{RAW}}$ images, but this time excluding all LUT elements with a 46° halo, corresponding to a halo ratio > 1 (cf. Fig 1)."

[1]For the sake of completeness, we provide here the ice crystal properties used for the DISORT simulations: Fig. 8b (SCF=80 %, r_{eff}=10μm), Fig. 9b (SCF=20 %, r_{eff}=10μm), Fig. 9e (SCF=20 %, r_{eff}=10μm), Fig. 9h (SCF=20 %, r_{eff}=10μm), Fig. 9k (SCF=80 %, r_{eff}=5μm), Fig. 9n (SCF=20 %, r_{eff}=10μm).

The LUT elements "with a 46 degree halo" are excluded, but how is this quantified?

LUT elements for which the 46° halo ratio is > 1 are excluded. We added this statement to the manuscript.

> "The retrieval was repeated for the individual HaloCam$_{\mathrm{RAW}}$ images excluding all LUT elements with a 46° halo, corresponding to a halo ratio > 1 (cf. Fig. 1)."

Minor comments:

Page 1, Line 21: add "be" between "to" and "more"

Done.

Page 2, line 4: add "to" after "helps"

Done.

Page 2, line 21: The papers van Diedenhoven et al. (2012, 2020) are cited referring to RSP data, but both papers use POLDER data. The van Diedenhoven et al. (2013) that is also in the reference list is using RSP data and could be cited here as well. The other two papers could be cited in the previous sentence, although "more recently" does not apply then anymore.

We corrected this section:

> "Multi-angular polarized reflectances from the Polarization and Directionality of Earth Reflectance (POLDER) have been used to infer information about ice crystal shape (e.g. Descloitres et al., 1998; Chepfer et al., 2001; Baran and Labonnote, 2006; Sun et al., 2006). More recently, POLDER observations have been used to retrieve ice crystal aspect ratio and distortion levels: van Diedenhoven et al. (2012, 2020); van Diedenhoven (2021) found that crystal distortion and aspect ratio increase with cloud top height, leading to decreasing asymmetry parameters. These studies mainly focus on tops of optically thick ice clouds."

Page 4, line 3-4: : ice crystal orientation also has significant effects on the global radiative budget (Noel and Sassen, 2005)". This is an overstatement and not supported by the cioted paper. Other studies, such as Breon and Dubrulle (https://doi.org/10.1175/JAS-3309.1) and Zhou et al. (https://doi.org/10.1175/JAMC- D-11-0265.1) have concluded that the percentage of oriented plates in the clouds is verry low and that "These low fractions imply that the impact of oriented plates on the cloud albedo is insignificant." Please correct the statement in the paper.

Thank you for the pointer. We removed this part of the statement:

> "While ice crystal orientation also has significant effects on the remote sensing of ice cloud properties, this study focuses on randomly oriented ice crystals for a start and leaves investigation of oriented crystals for a future study."

Page 5, line 9 and throughout the paper: The 8-element aggregate of columns is named "8-element columns" here, but this is confusing in my view. Please refer to this as an aggregate throughout the paper. Also correct the naming of the plate aggregates accordingly.

We corrected the naming in the abstract and conclusions as well as for the first time describing these crystal shapes, but refer to the short version throughout the main part of the manuscript for the sake of brevity. We added a note in the text:

> "Optical properties based on Yang et al. (2013) (referred to as YG13 in the following) were used for eight different habits: solid columns, hollow columns, plates, 8-element aggregate of columns, 5-element aggregate of plates, 10-element aggregate of plates, solid bullet rosettes, and hollow bullet rosettes, all of which are based on hexagonal crystal symmetry. Droxtals were not considered for the retrieval since they do not produce a 22° halo (Yang et al., 2013). For the sake of brevity, we will refer to the aggregates of columns and plates as 8-element columns, 5-element plates, and 10-element plates."

Page 5, line 26: A bias in what? Radiance, retrieved SCF? Please specify.

We clarified this statement:

> " Figure B3 in Appendix B shows that this causes a bias in the 22° halo radiances of 1.5% for the blue, 2.0% for the green, and 1.2% for the red channel."

Page 10, line 3: The grammar of this sentence does not seem to be correct.

Corrected.

> "For solid columns (Fig. 5a) the SCF peaks below 50% and HaloCam$_{\mathrm{RAW}}$'s 22° halo observations are represented best by a mean SCF of 35.9% and RCF of 64.1% (cf. Eq. 3)."

Page 10, line 35: Note that the base temperature of -10C is out of the range of your definition of cirrus.

Thank you for pointing this out. We corrected that statement:

> "In both the 2017 and the present study we refer to cirrus clouds as non-precipitating ice clouds. In the 2017 study, we even constrained the observations to cloud base temperatures of $-20\,^{\circ}\mathrm{C}$ or colder."

Page 14: figures 6 and 7 are out of order with the text.

We kept the order of figures 6 and 7 (now 8 and 9) but adjusted the order of reference in the text. This section now reads:

> "For analyzing this scattering angle region, we therefore use HaloCam$_{\mathrm{RAW}}$ observations averaged over each day and make use of the presence or absence of the 46° halo in a qualitative way to further constrain the retrieved ice crystal properties from Section 3.1. We focused this analysis on six of the eight days, for which the number of halo samples was high and the horizontal extent of the cirrus cloud was large enough to yield homogeneous conditions across both the 22° and 46° halo regions in the averaged image. If ice crystals in the cirrus cloud were able to form a 46° halo, we would expect to see it in the averaged image. Figure 8 displays the averaged HaloCam$_{\mathrm{RAW}}$ measurements for 22 September 2015 (a) in comparison with DISORT simulations (b) using ice crystal plates, which were found to best match the observations in the region of the 22° halo (cf. Table 3). "

References

Baran, A. J. and Labonnote, L. C.: On the reflection and polarisation properties of ice cloud, J. Quant. Spectrosc. Radiat. Transfer, 100, 41–54, https://doi.org/10.1016/j.jqsrt.2005.11.062, VIII Conference on Electromagnetic and Light Scattering by Nonspherical Particles, 2006.

Chepfer, H., Goloub, P., Riedi, J., De Haan, J. F., Hovenier, J., and Flamant, P.: Ice crystal shapes in cirrus clouds derived from POLDER/ADEOS-1, Journal of Geophysical Research, 106, 7955–7966, https://doi.org/10.1029/2000JD900285, 2001.

Descloitres, J., Buriez, J.-C., Parol, F., and Fouquart, Y.: POLDER observations of cloud bidirectional reflectances compared to a plane-parallel model using the International Satellite Cloud Climatology Project cloud phase functions, Journal of Geophysical Research, 103, 11 411–11 418, https://doi.org/10.1029/98JD00592, 1998.

Forster, L., Seefeldner, M., Wiegner, M., and Mayer, B.: Ice crystal characterization in cirrus clouds: a sun-tracking camera system and automated detection algorithm for halo displays, Atmos. Meas. Tech., 10, 2499–2516, https://doi.org/10.5194/amt-10-2499-2017, 2017.

Forster, L., Seefeldner, M., Baumgartner, A., Kölling, T., and Mayer, B.: Ice Crystal Characterization in Cirrus Clouds II: Radiometric Characterization of HaloCam for the Quantitative Analysis of Halo Displays, amtd, 2020.

Sun, W., Loeb, N. G., and Yang, P.: On the retrieval of ice cloud particle shapes from POLDER measurements, J. Quant. Spectrosc. Radiat. Transfer, 101, 435–447, https://doi.org/10.1016/j.jqsrt.2006.02.071, 2006.

van Diedenhoven, B.: Variation of Ice Microphysical Properties With Temperature and Humidity at Tops of Convective Clouds, Geophysical Research Letters, p. e2021GL093673, https://doi.org/10.1029/2021GL093673, e2021GL093673 2021GL093673, 2021.

van Diedenhoven, B., Fridlind, A. M., Ackerman, A. S., and Cairns, B.: Evaluation of Hydrometeor Phase and Ice Properties in Cloud-Resolving Model Simulations of Tropical Deep Convection Using Radiance and Polarization Measurements, J. Atmos. Sci., 69, 3290–3314, https://doi.org/10.1175/JAS-D-11-0314.1, 2012.

van Diedenhoven, B., Ackerman, A. S., Fridlind, A. M., Cairns, B., and Riedi, J.: Global Statistics of Ice Microphysical and Optical Properties at Tops of Optically Thick Ice Clouds, Journal of Geophysical Research: Atmospheres, 125, e2019JD031 811, https://doi.org/10.1029/2019JD031811, https://agupubs.onlinelibrary.wiley.com/doi/abs/10.1029/2019JD031811, e2019JD031811 2019JD031811, 2020.

Yang, P., Bi, L., Baum, B. A., Liou, K.-N., Kattawar, G. W., Mishchenko, M. I., and Cole, B.: Spectrally Consistent Scattering, Absorption, and Polarization Properties of Atmospheric Ice Crystals at Wavelengths from 0.2 to 100 μm, J. Atmos. Sci., 70, 330–347, https://doi.org/10.1175/JAS-D-12-039.1, 2013.